FORMATION-FLYING SAR RECEIVERS IN FAR-FROM-TRANSMITTER GEOMETRY: SIGNAL MODEL AND PROCESSING SCHEME

Gerardo Di Martino, Alessio Di Simone, Michele Grassi, Marco Grasso, Maria Daniela Graziano, Antonio Iodice, Antonio Moccia, Alfredo Renga, Daniele Riccio, Giuseppe Ruello

Università degli Studi di Napoli Federico II, Napoli, Italy

IGARSS 2021 - 2021 IEEE International Geoscience and Remote Sensing Symposium | 978-1-6654-0369-6/21/$31.00 ©2021 IEEE | DOI: 10.1109/IGARSS47720.2021.9554384

ABSTRACT

The paper focuses on the concept of a formation-flying synthetic aperture radar (FF-SAR) bistatic system composed of a set of compact, low-weight satellite receivers in close formation (within 1 km) placed in the same low-Earth orbit at large distance (about 100 km) from a transmitter. Each receiver is conceived to fit a 12-unit CubeSat. A signal model adapted to the proposed formation geometry is also presented, and a corresponding processing scheme to achieve range swath widening and signal-to-noise ratio (SNR) improvement is illustrated and discussed.

Index Terms— bistatic SAR, distributed SAR, formation-flying SAR, CubeSats.

1. INTRODUCTION

The formation-flying synthetic aperture radar (FF-SAR) has been introduced in the last decades to enable new operational modes exploiting a set of very compact, low-weight, satellite platforms carrying receivers that simultaneously collect the signal emitted by a single spaceborne transmitter and scattered by the scene under survey [1]-[5].

When an FF-SAR is considered working with a close formation of N receivers, the Signal-to-Noise Ratio (SNR) resulting from the coherent combination of the echoes collected by each receiver is up to N times the SNR of each individual receiver. Moreover, when more than one receiver is available, the pulse repetition frequency (PRF) of the transmitter can be relaxed to values that are significantly lower than the Doppler bandwidth of the illuminated scene. This allows the system to increase the swath width which can be observed without range ambiguities, i.e., to implement High-Resolution Wide-Swath (HWRS) techniques. At the same time, unambiguous reconstruction of the Doppler history is achieved in processing.

The above-mentioned FF-SAR features are used in this paper to enable FF-SAR operation by a fleet of very compact bistatic passive SAR receivers that are compliant with a realization by CubeSats and work in cooperation with a pre-existing monostatic SAR mission which is exploited as an illuminator of opportunity. Indeed, owing to the low SWAP (Size Weight And Power) characteristics of CubeSats platforms, low performance is achieved by each bistatic receiver as an isolated entity. Nonetheless, the FF-SAR principle, i.e., the relevant power gain and ambiguity suppression capabilities, guarantees that the entire cluster is able to deliver high quality bistatic images which can be made compliant with operational applications, provided that a sufficient number of receivers can be deployed.

We underline that the receivers' formation considered here follows the transmitter at large distance (about 100 km). This ensures that the functionalities of the transmitting platform (e.g., telemetry, tracking, and command) remain unaffected by the presence of the receiving formation. The price to be paid is the impossibility to coherently combine the monostatic image obtained by the transmitting sensor itself with those obtained by the passive receivers, and a complication of processing used to coherently combine the passive receivers' signals. In fact, the usually made assumption (see, e.g., [4]) that the transmitter-to-receiver baseline is much smaller than platform height must be relaxed. Therefore, we here also present a signal model adapted to the proposed formation geometry and a corresponding efficient processing scheme.

The remainder of this paper is organized as follows. Section 2 depicts the designed system architecture and the selected working modes. Section 3 presents a signal model suitable to implement the FF-SAR processing scheme which is than discussed in Section 4.

2. SYSTEM ARCHITECTURE

The proposed system is based on an opportunity illuminator which transmits microwave signals. Table 1 lists the parameters of the selected X-band transmitter [6]. The cluster of CubeSats is assumed to include several equal satellites. The cluster flies along the same orbit as that of the transmitter with a separation in mean anomaly leading to an along-track distance of about 100 km. Two working modes are considered, namely SNR improvement and HRWS imaging. For the considered working modes, the cluster of receivers can be assumed to work with CubeSats that are mainly separated in the along-track direction as in a train of satellites, e.g., by 50-100 m between two consecutive receivers. Other baseline components can be present owing to inaccuracy of the relative orbit control but also as a nominal condition to decouple the collision risk with the along-track formation design, according to the safe ellipse principle [7]. The extent of these components is shorter than a few tens of meters at most [4] to limit phase nuisance terms given by surface topography.

Table 1: Parameters of the selected illuminator of opportunity [6].

Parameter	***Value***
Orbit altitude	410 km
Orbit eccentricity	~ 0.001
Orbit inclination	~ 97°
Carrier Wavelength	0.031 m
Monostatic Resolution	3 x 3 m
Incidence Angle	20°- 40°
Peak Power	< 1 kW
Polarization	VV
Antenna Size	3.4 x 0.7

The design of each CubeSat is the result of a trade-off between the required performance and the current technological capabilities of those platforms. Specifically, considering a 0.5 m radius receiving circular aperture [8] characterized by an efficiency of 0.6, radar equation can be used to compute the minimum number of receivers able to guarantee the same SNR of the transmitter. Based on Table 1, this minimum number corresponds to just three receivers.
As far as the HRWS mode is concerned, the standard SAR chronogram can be used to characterize, even though qualitatively, the effect of the PRF on the imaging performance. As illustrated in Figure 1, the magenta line corresponds to the PRF value of about 5400 Hz which is used by the transmitter for its monostatic operation and guarantees a maximum swath width of less than 30 km. A PRF reduction to about 2800 Hz (see Figure 1, black line), enables an extension of the swath width up to 60 km, but it leads to an undersampling of the Doppler bandwidth by a factor of two. So, two bistatic receivers are required, at least, to achieve unambiguous signal reconstruction. Finally, the unambiguous swathwidth reaches 100 km for a PRF of less than 1800 Hz (red line in Figure 1). Three receivers can be equipped with suitable antennas [8] to cover this extremely wide swath. More receivers could be necessary, together with proper system timing [9]-[10], to mitigate the effects of unavoidable errors in the sensors positioning.

3. SIGNAL MODEL

The geometry of the proposed FF-SAR is schematically depicted in Figure 2: one transmitter and N receivers move on the same track with constant velocity v. The transmitter position is $x'=vt$, and the i-th receiver position is $x_i'=x'-d+\Delta x_i$ (with $\Delta x_1=0$). The azimuth coordinate of the generic ground point is x, and its distance from the line of flight is r, see Figure 3. The transmitter operates in stripmap mode and the azimuth footprint of the transmitted beam is X_t. The receivers' antennas are pointed toward the illuminated scene and their beams are wider than the one of the transmitting antenna, so that their footprints include the illuminated area. The transmitter emits pulses at times $t_n=n/\mathrm{PRF}$, where PRF is the pulse repetition frequency. We assume that Δx_i and X_t are much smaller than the distance r of the generic ground point from the line of flight, whereas d may be of the same order of magnitude of r.

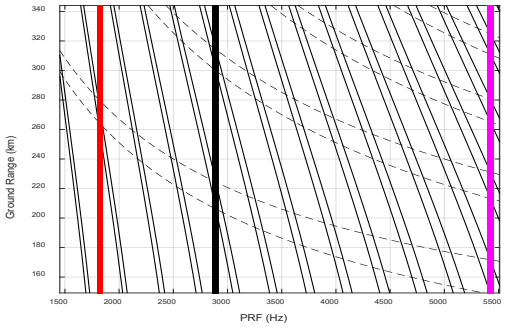

Figure 1: SAR chronogram corresponding to the parameters of Table 1: magenta line is the nominal monostatic PRF, black and red lines represent PRF reductions able to guarantee an extension of the swath up to 60 km and 100 km, respectively.

We assume that range processing of individual receivers' signals has been performed. In addition, although this is not necessary, to simplify notation and to focus on the method of combination of signals received by the different sensors, we ignore the problem of range migration correction. The signal received by the i-th sensor can be then expressed as

$$s_i(x',r)=\int \gamma(x,r)\, g_i(x'-x,r)\, dx + n_i(x',r) \quad , \tag{1}$$

where $\gamma(x,r)$ is the ground point bistatic reflectivity, $n_i(x',r)$ is the i-th receiver noise,

$$g_i(x'-x,r)=\exp\left[-j\frac{2\pi}{\lambda}(r_t+r_i)\right] w\left(\frac{x'-x}{X_t}\right) \quad , \tag{2}$$

$w(\cdot)$ is the product of the transmitting and receiving antenna patterns, which is assumed approximately unitary if the modulus of its argument is smaller than 0.5 and negligible otherwise, and r_t and r_i are the distances of the ground point from the transmitter and from the i-th receiver, respectively, see Figure 3. These distances can be computed as

$$r_t=\sqrt{r^2+(x'-x)^2}\cong r+\frac{(x'-x)^2}{2r} \quad , \tag{3}$$

$$r_i=\sqrt{r^2+(x'-d+\Delta x_i-x)^2}\cong$$
$$\cong \frac{r}{\cos\psi}-\sin\psi\,(x'-x+\Delta x_i)+\cos^3\psi\,\frac{(x'-x+\Delta x_i)^2}{2r} \quad , \tag{4}$$

where $\cos\psi=\dfrac{r}{\sqrt{r^2+d^2}}$ and $\sin\psi=\dfrac{d}{\sqrt{r^2+d^2}}$, (5)

ψ being the first receiver squint angle, see Figure 3. After some algebraic manipulation, we get

$$r_t+r_i\cong\frac{1+\cos\psi}{\cos\psi}r-\sin\psi\left(x'-x+\frac{\cos^3\psi}{1+\cos^3\psi}\Delta x_i\right)+$$
$$+\frac{1+\cos^3\psi}{2r}\left(x'-x+\frac{\cos^3\psi}{1+\cos^3\psi}\Delta x_i\right)^2+ \quad . \tag{6}$$
$$-\frac{\sin\psi}{1+\cos^3\psi}\Delta x_i+\frac{\cos^3\psi}{1+\cos^3\psi}\frac{\Delta x_i^2}{2r}$$

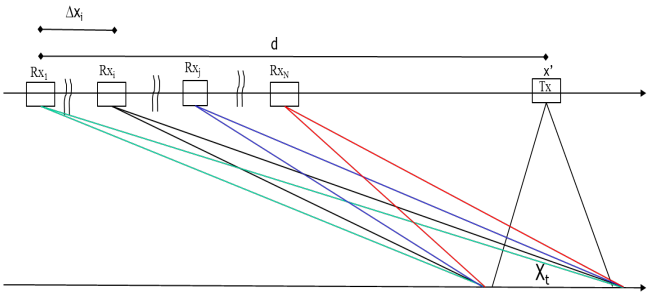

Figure 2: Geometry of the formation-flying SAR

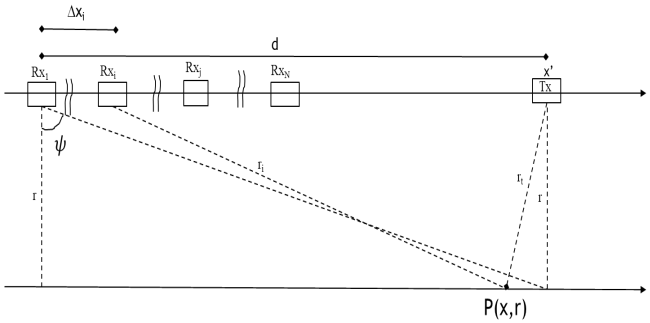

Figure 3: Definition of distances and squint angle.

By replacing (6) in (2), performing the Fourier Transform (FT) of (1) and provisionally treating x' as a continuous variable we get, after a stationary-phase evaluation of the Fourier integral,

$$S_i(\xi,r) = D(\xi,r) H_i(\xi,r) + N_i(\xi,r) \quad , \tag{7}$$

where ξ is the Fourier mate of x',

$$D(\xi,r) = \Gamma(\xi,r) G(\xi,r) \quad , \tag{8}$$

$$G(\xi,r) = \exp\left(j \frac{\xi^2}{4a} \right) \exp\left(-j \frac{\xi \pi}{\lambda a} \sin\psi \right) \quad , \tag{9}$$

$$H_i(\xi,r) = \exp\left(j\xi \tfrac{\cos^3\psi}{1+\cos^3\psi} \Delta x_i \right) \exp\left(j \tfrac{2\pi}{\lambda} \tfrac{\sin\psi}{1+\cos^3\psi} \Delta x_i \right) \cdot$$
$$\cdot \exp\left(-j \tfrac{\pi}{\lambda r} \tfrac{\cos^3\psi}{1+\cos^3\psi} \Delta x_i^2 \right) w\left[\frac{\xi - \frac{2\pi}{\lambda}\sin\psi + 2a \frac{\cos^3\psi}{1+\cos^3\psi} \Delta x_i}{2aX_t} \right] \quad , \tag{10}$$

$$a = \frac{\pi\left(1+\cos^3\psi\right)}{\lambda r} \quad , \tag{11}$$

and Γ and N_i are the FTs of γ and n_i. Since the signal in (1) is sampled at spatial frequency $\xi_s = 2\pi\mathrm{PRF}/v$, the actual FT $\tilde{S}_i$ of (1) is the superposition of replicas of (7), spaced by ξ_s. If $\xi_s \geq 2aX_t/M$, i.e., the PRF is greater than $1/M$ the Doppler bandwidth, then only M replicas are non-negligible, so that

$$\tilde{S}_i(\xi,r) = \sum_{j=1}^{M} S_i(\xi - j'\xi_s, r) = \sum_{j=1}^{M} H_{ij}(\xi,r) D_j(\xi,r) + \tilde{N}_i(\xi,r), \tag{12}$$

where $-\xi_s/2 \leq \xi \leq \xi_s/2$, $j' = j - \frac{M+1}{2}$ for M odd ,
or $0 \leq \xi \leq \xi_s$, $j' = j - \frac{M}{2}$ for M even ,

$$\begin{aligned} H_{ij}(\xi,r) &= H_i(\xi - j'\xi_s, r) \\ D_j(\xi,r) &= D(\xi - j'\xi_s, r) \\ \tilde{N}_i(\xi,r) &= \sum_{j=1}^{M} N_i(\xi - j'\xi_s, r) \end{aligned} \quad . \tag{13}$$

Equation (12) can be expressed in matrix form as

$$\underline{\tilde{S}}(\xi,r) = \underline{\underline{H}}(\xi,r) \underline{D}(\xi,r) + \underline{\tilde{N}}(\xi,r) \quad , \tag{14}$$

where $\underline{\tilde{S}}(\xi,r)$ and $\underline{\tilde{N}}(\xi,r)$ are N-element column vectors, $\underline{D}(\xi,r)$ is an M-element column vector, and $\underline{\underline{H}}(\xi,r)$ is an N-row-by-M-column matrix.

4. PROCESSING SCHEME

The obtained expression (14) is similar to the one presented for instance in [4], so that a similar processing scheme can be devised to remove ambiguity and increase SNR: assuming $M \leq N$, $\underline{D}(\xi,r)$ can be estimated as

$$\underline{\hat{D}}(\xi,r) = \underline{\underline{H^{\dagger}}}(\xi,r) \underline{\tilde{S}}(\xi,r) \quad , \tag{15}$$

where $\underline{\underline{H^{\dagger}}} = \left(\underline{\underline{H^*}}\, \underline{\underline{H}} \right)^{-1} \underline{\underline{H^*}}$ is the pseudo inverse of $\underline{\underline{H}}$, and $\underline{\underline{H^*}}$ is its transpose conjugate. The unfolded unambiguous spectrum of $\hat{D}(\xi,r)$ is then reconstructed by disposing the elements of the vector $\underline{\hat{D}}(\xi,r)$ over the ξ axis, with $-M\xi_s/2 \leq \xi \leq M\xi_s/2$, see Figure 4. Finally, the output unambiguous SAR image $\hat{\gamma}(x,r)$ is obtained by resorting to usual monostatic SAR processing, i.e.,

$$\hat{\gamma}(x,r) = FT^{-1}\left\{ G^*(\xi,r) \hat{D}(\xi,r) \right\} \quad . \tag{16}$$

However, a significant difference is present: eq.(6) shows that the equivalent phase center displacement of the i-th sensor is

$$\Delta\bar{x}_i = \frac{\cos^3\psi}{1+\cos^3\psi} \Delta x_i \quad , \tag{17}$$

which is slightly range-dependent and reduces to the usual form $\Delta\bar{x}_i = \Delta x_i/2$ only if d vanishes. Accordingly, the ideal positions of sensors, for which maximum SNR improvement

(equal to a factor of N) and maximum ambiguity reduction are obtained, differ from those of [4], [9] and are:

$$\Delta x_i = \frac{1+\cos^3\psi}{\cos^3\psi}\frac{v}{PRF}\left(\frac{i-1}{N}+k_i\right) \quad , \tag{18}$$

with k_i integers. Note that if Δx_i is of the order of 100 m, even a variation with respect to 0.5 in the multiplicative coefficient in (17) as small as 0.02 (as it is obtained for d = 100 km and r = 500 km, corresponding to the system of Table 1 with ϑ=35°) gives significant phase variations in the exponentials in (10), so that it cannot be neglected.

For M>1 the presented processing scheme allows achieving both HRWS and SNR improvement. If the PRF is greater than the Doppler bandwidth, then we can set M=1, and it can be verified that processing in (15-16) simply leads to the coherent summation of the properly rephased images obtained by the individual sensors, thus leading to SNR improvement.

Finally, as noted in [4],[9]-[10], uncertainty on the relative sensor orbit control is larger than the distance between ideal sensor positions of (18) and "bad" positions, so that we may obtain an ill-conditioned $\underline{\underline{H}}^*\underline{\underline{H}}$ matrix and hence significant ambiguity and reduced SNR. The probability density function (pdf) of the condition number (CN) of $\underline{\underline{H}}^*\underline{\underline{H}}$, i.e., the ratio of the largest over the smallest of its eigenvalues, can be computed by assuming that phases $\xi_s \Delta x_i$ are independent random variables uniformly distributed in $-\pi,\pi$. This pdf is plotted in Figure 5 for M=2 and for different values of N. It turns out that, for M=2, the probability that CN<10 (so that a sufficiently well-conditioned matrix is obtained [4]) is 0.61, 0.84, 0.93, 0.97 and 0.99 for N varying from 2 to 6. However, for a given set of sensor positions, CN can be reduced by proper selection of the PRF, with the same procedure as in [9].

5. CONCLUSION

The concept of an FF-SAR with large transmitter-to-receiver baseline has been considered, and a proper signal model and corresponding processing algorithm have been proposed. Robustness of the approach with respect to unavoidable sensors positioning errors has been explored.

6. ACKNOWLEDGMENTS

This work has been supported by the Italian Ministry of University and Research through the project "FORmation flying of CubEsat assemblies for remote sensing (FORCE)".

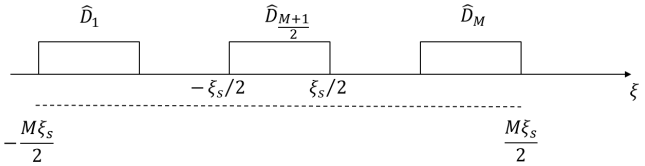

Figure 4: Unfolded spectrum reconstruction (case of odd M).

7. REFERENCES

[1] N. A. Goodman, J. M. Stiles, "Resolution and Synthetic Aperture Characterization of Sparse Radar Arrays," *IEEE Trans. Aerosp. Electron. Syst.*, vol. 39, no. 3, pp. 921-935, 2003.

[2] J. P. Aguttes, "The SAR train concept: an along-track formation of SAR satellites for diluting the antenna area over N smaller satellite, while increasing performance by N", *Acta Astronautica*, Vol. 57, pp. 197-204, 2005.

[3] G. Krieger, A. Moreira, "Spaceborne bi- and multistatic SAR: Potential and challenges," *Proc. Inst. Elect. Eng.-Radar, Sonar Navig.*, vol.153, no. 3, pp. 184–198, Jun. 2006.

[4] P. Guccione, A. Monti Guarnieri, F. Rocca, D. Giudici, N. Gebert, "Along-Track Multistatic Synthetic Aperture Radar Formations of Minisatellites," *Remote Sens.,* Vol. 12, No. 12, 2020.

[5] A. Renga, M. D. Graziano and A. Moccia, "Formation Flying SAR: analysis of imaging performance by Array Theory," *IEEE Trans. Aerosp. Electron. Syst.*, doi: 10.1109/TAES.2020.3043526, 2020.

[6] V. Stanzione, B. Sabatinelli, "Platino Project: A new Italian multi-application small satellite platform for highly competitive missions", *69th International Astronautical Congress*, October 2018.

[7] M. Grasso, A. Renga, G. Fasano, M.D. Graziano, M. Grassi, A. Moccia, "Design of an end-to-end demonstration mission of a Formation-Flying Synthetic Aperture Radar (FF-SAR) based on microsatellites," *Advances in Space Research*, 15 pp., May 2020.

[8] G. Di Martino, A. Di Simone, M. Grassi, M. Grasso, M. D. Graziano, A. Iodice, A. Moccia, A. Renga, D. Riccio, G. Ruello, "Formation-Flying SAR Receivers in Far-From-Transmitter Geometry: X-Band SAR Antenna Design", *IGARSS 2021 – 2021 IEEE Int. Geosci. Remote Sens. Symp.*, Brussels, July 2021.

[9] M. D. Graziano, A. Renga, M. Grasso, A. Moccia, "PRF Selection in Formation-Flying SAR: Experimental Verification on Sentinel-1 Monostatic Repeat-Pass Data," *Remote Sens.,* Vol. 12, No. 29, 2020.

[10] A. Renga, M. D. Graziano, M. Grasso, A. Moccia, "Timing and Design Issues in Formation Flying Distributed SAR," *IEEE Radar Conference*, 6 pp., Sept. 2020.

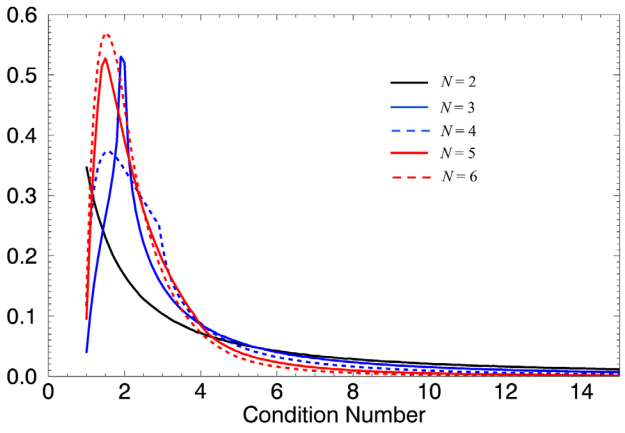

Figure 5: pdf of the condition number (CN) of $\underline{\underline{H}}^*\underline{\underline{H}}$ for M = 2 and N varying from 2 to 6. The probability that CN<10 is 0.61, 0.84, 0.93, 0.97 and 0.99 for N varying from 2 to 6.